Paper IV

Inline SAW RFID tag using time position and phase encoding

S. Härmä, W. G. Arthur, C. S. Hartmann,
R. G. Maev, and V. P. Plessky

IV

S. Härmä, W. G. Arthur, C. S. Hartmann, R. G. Maev, and V. P. Plessky, "Inline SAW RFID tag using time position and phase encoding", IEEE Transactions on Ultrasonics, Ferroelectrics, and Frequency Control, Vol. 55, No. 8, August 2008, pp. 1840-1846.

Inline SAW RFID Tag Using Time Position and Phase Encoding

Sanna Härmä, Wesley G. Arthur, *Student Member, IEEE*, Clinton S. Hartmann, *Member, IEEE*, Roman G. Maev, *Senior Member, IEEE*, and Victor P. Plessky, *Senior Member, IEEE*

***Abstract*—Surface acoustic wave (SAW) radio-frequency identification (RFID) tags are encoded according to partial reflections of an interrogation signal by short metal reflectors. The standard encryption method involves time position encoding that uses time delays of response signals. However, the data capacity of a SAW RFID tag can be significantly enhanced by extracting additional phase information from the tag responses.**

In this work, we have designed, using FEM-BEM simulations, and fabricated, on 128°-$LiNbO_3$, inline 2.44-GHz SAW RFID tag samples that combine time position and phase encoding. Each reflective echo has 4 possible time positions and a phase of 0°, −90°, −180°, or −270°. This corresponds to 16 different states, i.e., 4 bits of data, per code reflector. In addition to the enhanced data capacity, our samples also exhibit a low loss level of −38 dB for code reflections.

I. Introduction

The encoding of surface acoustic wave (SAW) radio-frequency identification (RFID) tags is based on partial reflections of an interrogation signal from short metal reflectors. The standard encryption method, time position encoding, uses time delays of response signals. The physical positions of the code reflectors on the chip surface determine the time delays of the reflective echoes and thus the time-delay-based code carried by the response signal. However, the data capacity of a SAW RFID tag can be significantly enhanced if the phases of the reflective echoes are also used for encoding.

In this work, we have designed, using FEM-BEM simulations, and fabricated, on 128°-$LiNbO_3$, inline 2.44-GHz SAW RFID tag samples that combine time position and phase encoding. For time position encoding, each reflector has 4 possible positions, corresponding to 2 bits of data. In addition, a phase shift of 0°, −90°, −180°, or −270° is introduced, yielding an additional 2 bits of data per reflector. In addition to the enhancement of data capacity, we have also kept in mind the importance of reducing the signal loss because this is related to the increase of the tag read range.

In the following sections, we first introduce the geometry and the encoding principles of the SAW RFID tags designed in this work, and then we describe the methods used in the analysis of simulated and measured tag responses. Finally, we present the results of extracting the phase-based codes carried by our tag samples.

Manuscript received November 26, 2007; accepted February 18, 2008. S. Härmä thanks the Foundation of Technology (Finland), the Nokia Foundation, and the Finnish Foundation for Economic and Technology Sciences (KAUTE) for postgraduate scholarships.

S. Härmä and V. P. Plessky are with the Department of Engineering Physics, Helsinki University of Technology, Finland (e-mail: sanna.harma@tkk.fi).

V. P. Plessky is also with GVR Trade SA, Bevaix, Switzerland.

W. G. Arthur and R. G. Maev are with the Department of Physics, University of Windsor, Ontario, Canada.

C. S. Hartmann is with RF SAW Inc., Richardson, TX.

Digital Object Identifier 10.1109/TUFFC.2008.867

II. Tag Samples

We have designed and fabricated 2 sets of inline tags. For one set, encoding is based only on the time positions of reflective echoes; for the other, combined time position and phase encoding is used. All devices use a single-phase unidirectional transducer (SPUDT) [1] allowing for a size reduction of about 3 mm, as compared with a tag having a standard bidirectional interdigital transducer (IDT). The SPUDT is very similar to that used in [2] and consists of a reflector section of open-circuited electrodes sandwiched by 2 identical transducer sections. Each tag sample also has 14 short metal reflectors at precisely determined positions, as illustrated in Fig. 1. The first and the last reflector are at fixed positions (the same for all studied samples) and are used for time position calibration. The remaining 12 reflectors are used for encoding such that 10 of them form the code itself and 2 create a checksum for error control purposes. Each reflector consists of a small number of open-circuited electrodes. The reflector strengths are selected so as to ensure uniform amplitudes of reflected pulses [3], [2]. Reflectivity is gradually increased along the reflector array by increasing the number of electrodes in a reflector and by adjusting the metal ratio. The weakest reflectors, situated in the beginning of the code reflector array, only have one electrode. The SPUDT as well as the reflectors have the same internal geometry for all the studied samples; only the positions of the code and checksum reflectors are varied.

A. Time Position and Phase Encoding

For time position encoding, we use the encoding scheme already presented in [2] where a 125-ns time window is reserved for each code reflector (including the checksum reflectors). As shown in Fig. 2, this time window is divided into five 25-ns slots, one of the first 4 of which is occupied by a reflector. In other words, each reflector has 4 pos-

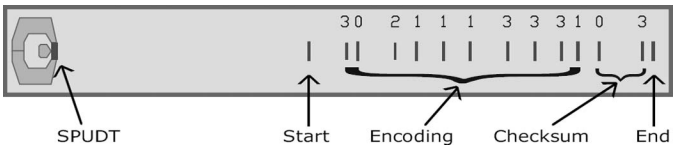

Fig. 1. General geometry of tag samples. Start and End reflectors are used for calibration. Chip size is 6.1 mm by 0.7 mm.

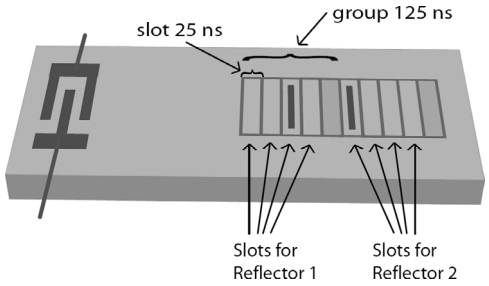

Fig. 2. Principle of time position encoding. Schematic drawing.

sible positions, corresponding to 2 bits of data. The total data capacity of our time-delay-based tags, having 10 code reflectors each, is thus 20 bits. However, a significant enhancement of data capacity can be achieved by combining time position encoding with phase encoding.

In this work, we present an encoding method that uses both the time delay and phase information of reflected pulses. This scheme consists of placing the reflectors more precisely within their slots. We introduce phases of 0°, −90°, −180°, and −270° by shifting the reflector positions by multiples of $\lambda/8$, as depicted in Fig. 3. When the combined time position and phase encoding is used, each reflector has 4 possible time positions and 4 possible phases. This sums up to 16 different states and corresponds to 4 bits of data. The 10-code-reflector tag then has a data capacity of 40 bits.

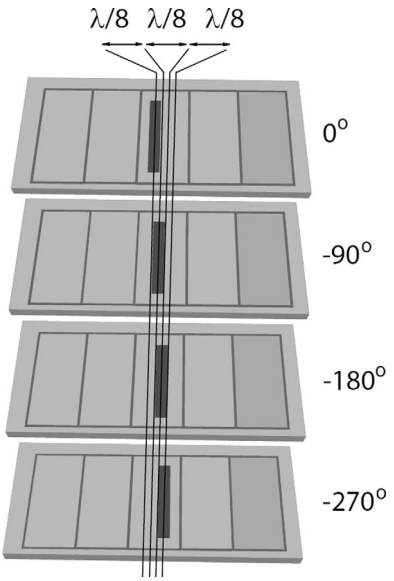

Fig. 3. Principle of phase encoding. Proportions are not correct.

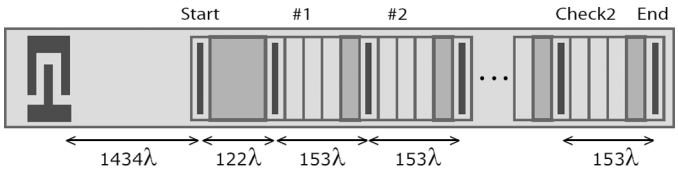

Fig. 4. Reflector positions for the first slot in a group. Applies to all studied tag samples.

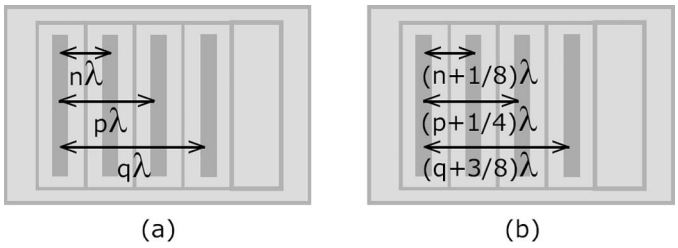

Fig. 5. Possible reflector positions for (a) time position encoding and (b) combined time position and phase encoding; n, p, and q are integers.

B. Encoding Principles of Tag Samples

As mentioned above, we have designed and fabricated 2 sets of tags, one with time position encoding only, the other with combined time position and phase encoding. Each set includes 11 tags and 11 different codes. To facilitate comparisons of results between these 2 tag types, we have set the phases for the first position in each group as 0°, as illustrated in Fig. 4. This applies to both the time-position-encoded tags and the tags using the combined encoding method. Moreover, all reflector positions for the time-position-encoded tags lie at multiples of λ from each other, as illustrated in Fig. 5(a), and correspond to a phase of 0°, although phase information does not play any role in time position encoding. We have also paired the tags such that for each time-position-encoded tag, there is a tag using the combined method with the same code. Moreover, the tag using the combined method carries the same code in reflector positions as in phases. Hence, a reflector placed at the second slot of a group always has a phase of −90°. The third and fourth slots correspond to −180° and −270°, respectively. Fig. 5(b) illustrates this encoding principle. In this way, although not using the full encoding capacity of the tag, we are able to compare the phases with those of the time-position-encoded counterpart. In practice, the codes based on time delays and those based on phases are naturally independent of each other, and each reflector truly has 16 different states.

III. Analysis of Tag Responses

We numerically study tag responses to a 25-ns-long Gaussian-shaped pulse (f_c = 2450 MHz) using S parameters obtained from measurements and FEM-BEM simulations. The simulations were carried out using FEMSAW

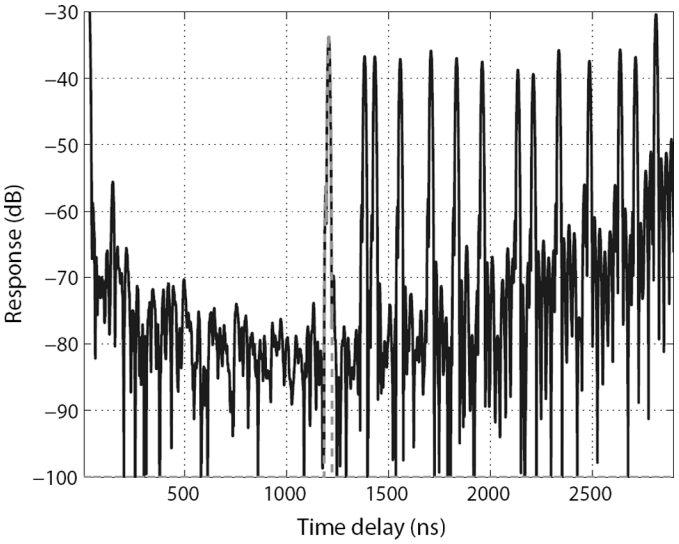

Fig. 6. Time response of a tag sample. Experimental data. (Dashed curve shows the time-gated Start pulse.)

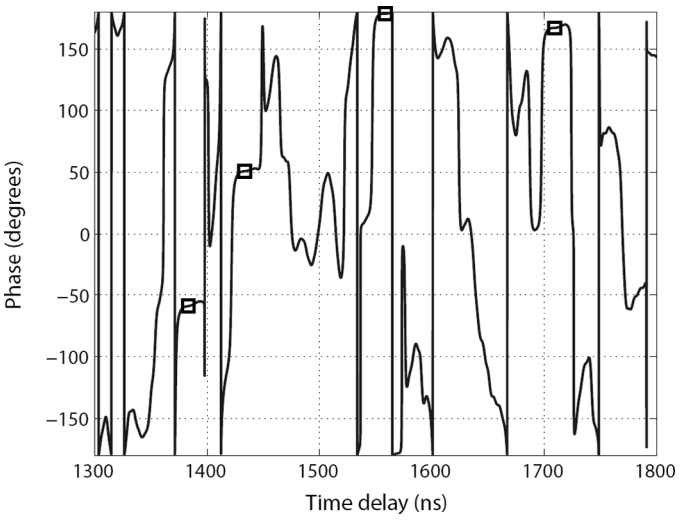

Fig. 7. Phase of response signal for a tag sample. Reflections from code reflectors are indicated by squares. Experimental data.

software (GVR Trade SA, Bevaix, Switzerland) [4]. The frequency range used in simulations and measurements spans 2250 MHz to 2650 MHz with a step of 0.25 MHz. This range gives a time resolution of $\Delta T = 2.5$ ns and a time window of $T = 4$ μs. However, this resolution is not adequate for studying the phases of the reflected pulses because one period of a surface acoustic wave is as short as 0.4 ns. For this reason, we enhance the time resolution by artificially extending the frequency range down to 0 Hz and up to 40 GHz by replacing the acoustic part of S_{11} with very small values. A 40-GHz range corresponds to a time step of $\Delta T = 0.025$ ns and allows us to determine phases with sufficient accuracy. Fig. 6 presents a typical experimental time response for a sample. As can be seen, the loss level, i.e., the ratio of the amplitudes of the code reflections to the amplitude of the interrogation signal, is about -38 dB. For comparison, an insertion loss of -53 dB was achieved for the weakest code reflections in [3]. The difference is due to the fact that we have used a unidirectional transducer and carefully optimized the structure of the reflector array.

A. Time Position and Phase Decoding

For all tags, the time positions of code reflections are easily and reliably attributed to a code sequence by first locating the "Start" and "End" calibration reflections, then dividing the time span in between into an appropriate number of slots and groups, and finally determining for each group the slot that corresponds to the local maximum of the response signal.

To extract the phase information of the reflected pulses, we divide the time response by a reference signal of the form $e^{j\omega_c t}$, where ω_c refers to the center frequency of the interrogation pulse. In this way, the phase of the response signal is compared with that of the reference signal, and the reflections from code reflectors are expected to be represented by segments of constant phase. Fig. 7 shows the extracted phases as a function of time for a section of the time window. The reflections from the code reflectors are indicated by squares. As can be seen, the phases do not remain constant within the duration of reflection but instead exhibit a gradual increase. Because this phenomenon can hardly be attributed to interactions with the wide-band short metal reflectors or to propagation on the chip surface, it is suggested that this anomaly has its origin in the SPUDT.

B. Phase Distortion Due to SPUDT

To study the possible phase distortions caused by the SPUDT, we analyze experimental S_{21} data of a delay line consisting of 2 such SPUDTs facing each other and separated by $L = 4$ mm. For loss considerations, Fig. 8 shows the absolute value of the S_{21} parameter of the delay line. The minimum insertion loss is -11.3 dB. However, about -5.8 dB should be attributed to propagation losses, which leaves -5.5 dB for the SPUDT losses. The dashed line in Fig. 9 presents the (unwrapped) phase of S_{21} after time-gating the direct signal from one SPUDT to the other. This line represents the phase $\varphi = -2\pi fL/v$, where v is the SAW velocity. However, fitting a linear function to these phase data for the range 2375 MHz to 2520 MHz and subtracting it from the original data reveals that the SPUDTs indeed are responsible for a phase distortion of up to several degrees depending on the frequency. This phase distortion is presented by the solid curve in Fig. 9. When only 4 different phases are used for encoding, this phase error is not very critical. However, data capacity may be enhanced by using a phase difference far smaller than the 90° used in this work. Then, a reliable extraction of phase-based codes requires eliminating the phase distortion caused by the SPUDT.

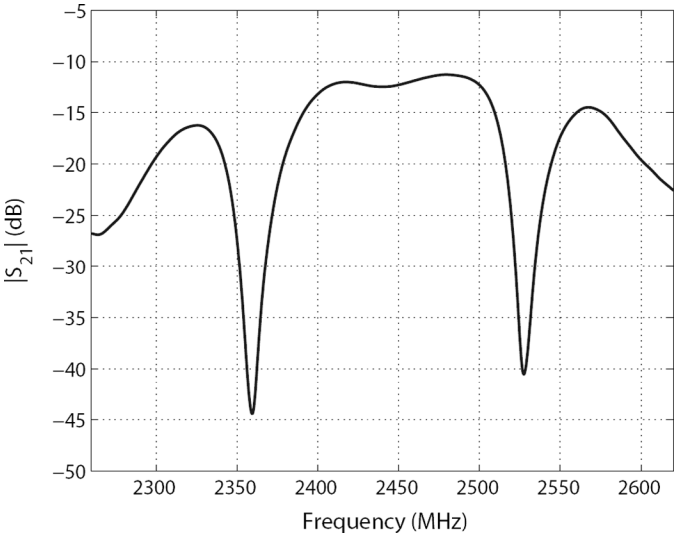

Fig. 8. $|S_{21}|$ for a delay line consisting of 2 SPUDTs facing each other and separated by 4 mm. Experimental data.

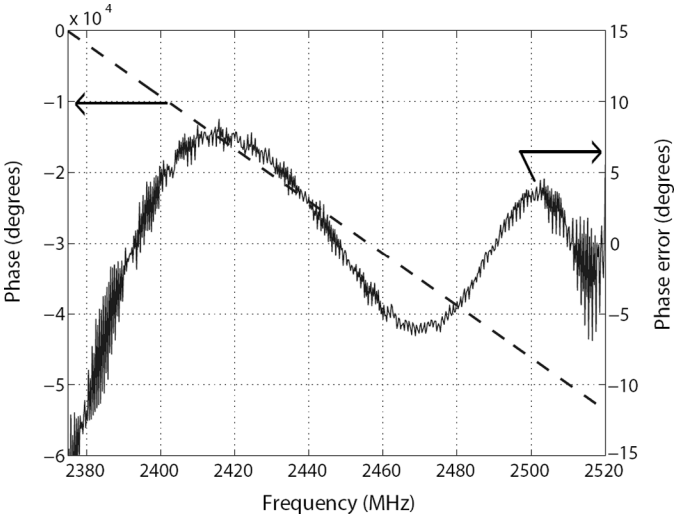

Fig. 9. Phase of S_{21} (dashed) for a delay line consisting of 2 SPUDTs and phase distortion (solid) due to SPUDTs. Experimental data.

C. Elimination of Phase Distortion Due to SPUDT

Each reflective echo includes a contribution from the SPUDT, the free-surface propagation, the reflector at which the reflection has occurred, and all the reflectors preceding that reflector. If we denote the initial signal received by the tag by S_0, then the kth reflected signal can be written as

$$S_k = S_0 D^2 R_k \prod_{i=1}^{k} P_i^2 \prod_{i=1}^{k-1} T_i^2, \tag{1}$$

where D includes the amplitude and phase distortion due to the SPUDT, P_i refers to the free-surface propagation between the ith and $(i-1)$th reflector (here $i=0$ corresponds to the SPUDT), T_i is the transmission coefficient of the ith reflector, and R_k is the reflection coefficient of the

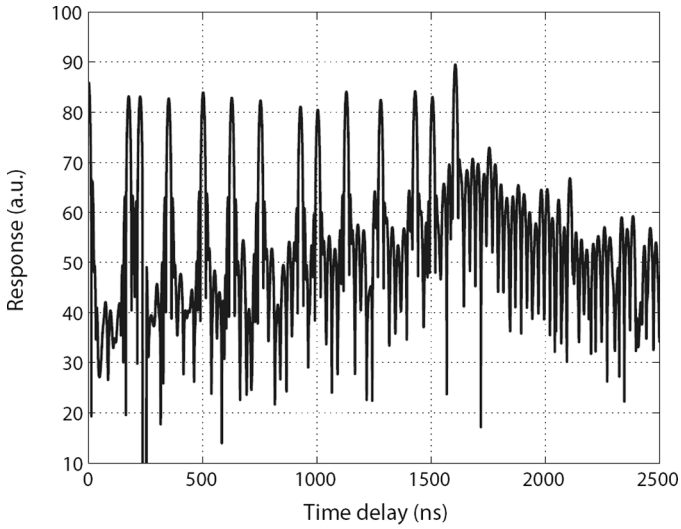

Fig. 10. Time response after elimination of SPUDT effects.

kth reflector. Eq. (1) hence only applies to the direct reflections from code reflectors and does not consider multiple reflections between reflectors. All the quantities appearing in (1) are complex-valued and frequency-dependent. In particular, the reflection from the first reflector (the Start reflector) has the form

$$S_1 = S_0 D^2 P_1^2 R_1. \tag{2}$$

In the Matlab (MathWorks, Natick, MA) routines that we use for analysis, the products in (1) and (2) are calculated pointwise at each frequency.

Now, we use (1) and (2) to eliminate the effect of SPUDT by dividing the total tag response by the first reflection. Hence, the received signal S_0, transducer contribution D^2, (round-trip) propagation between the IDT and the first reflector P_1^2, and the reflection from the first reflector R_1 are eliminated from each reflection. This elimination is achieved by first time-gating the Start pulse from the total time response (dashed curve in Fig. 6), then transforming the time-gated signal into the frequency domain and dividing the total frequency response by the time-gated signal, and finally by weighting the result of the division and transforming it back to the time domain. The result is seen in Fig. 10; the signal level after this manipulation is of course arbitrary. Due to the elimination of the propagation between the transducer and the first reflector, the peaks have shifted such that the first reflection is now observed at 0 ns. Phase extraction from the response signal now results in flat line segments as shown in Fig. 11.

Phase distortion of SPUDTs has recently been studied in [5].

D. Phase Corrections

To read the phase-based codes, 2 corrections are required: first, a design-time simplification related to the phase shifts at reflections from and transmissions through

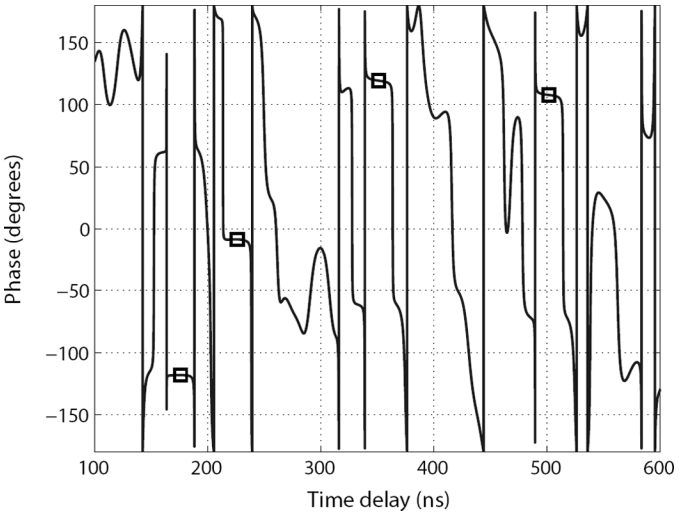

Fig. 11. Phase of response signal after elimination of SPUDT effects.

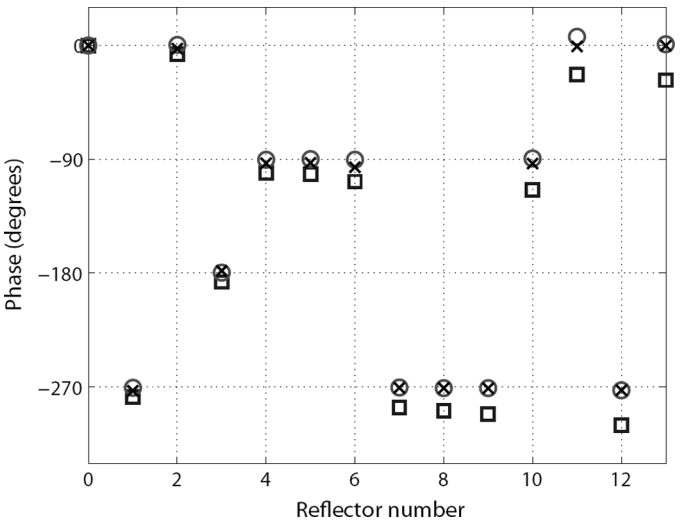

Fig. 12. Difference of phases for a time-position-encoded tag and a phase-encoded tag. Circles: simulated data without phase corrections; squares: experimental data without phase corrections; crosses: experimental data with phase corrections.

the code reflectors must be compensated for, and second, the difference in the SAW velocity and frequency between design and measurement, as well as the change in distances due to temperature variations, must be taken into account.

In design, we ignored the phase shifts due to reflection and transmission which, especially for later reflections that already include effects associated with transmission through many reflectors, play a significant role. However, we have determined these phase shifts for each reflector individually through numerical experiments similar to those reported in [6]. We have used FEMSAW for these simulations. The obtained phase shifts have been used as correction angles when analyzing the tag responses.

In design, we assumed that the SAW velocity on 128°-$LiNbO_3$ was 3978.48 m/s and used the center frequency 2441.75 MHz of the ISM band. This corresponds to a wavelength of 1.629 μm, which was used to determine the positions of the reflectors and hence to yield the desired phases for the reflected signals. However, both the velocity assumed in FEMSAW and the actual real-world velocity are different from that assumed in the design. Although small, this difference is sufficient to bring about significant phase changes. Also, while the design was made for a single frequency point, the actual device must be decodable for a full range of frequencies within the operating band. The observed wavelength is thus usually not equal to the wavelength assumed in design. The distances between the SPUDT and the reflectors also vary with temperature changes. To compensate for these effects, all extracted phase data must be weighted accordingly using a linear calibration function (linear dependency on time delay).

To determine the slope of the linear correction, we compare the number of wavelengths corresponding to a short distance on chip for both design and experiment. The experimental value is obtained from

$$N_\lambda = f_c \Delta t, \tag{3}$$

where f_c is the center frequency of the interrogation pulse and Δt is the experimentally observed time delay corresponding to the short distance. In principle, accurate analysis requires 2 reflectors (preferably the first 2 in the array) to lie sufficiently close to each other. In particular, their separation must be such that the difference between designed and experimental total phases corresponding to this distance does not exceed 2π. If this is the case, phase ambiguity is avoided and the slope of the linear phase correction can be obtained as the ratio of the difference between the experimental and designed phases with the time delay corresponding to the short distance in question. Because our design does not include such short distances, we have used the difference of 2 similar distances to obtain a sufficiently short distance. Similar methods for interpretation of phase data were proposed in [7] and [8].

In the future, the phase shifts at reflection and transmission must be included in the design, and the separation of the first 2 reflectors must be short and fixed.

IV. Results

The phase data presented in Fig. 12 are related to a pair of tag samples having the same code. One of these tags uses time position encoding only (and is designed to have equal phases for all reflections), and the other uses combined time position and phase encoding. Fig. 12 presents the difference of phases for each reflection for these 2 samples, both for measured (squares) and simulated cases (circles). For simulated data, phase encoding works almost ideally, and the measured phase data can also be interpreted without ambiguity. This kind of phase comparison for a pair of tags corresponds to the use of a reference tag with known constant phases in conjunction with a phase-encoded tag having an unknown code. No phase corrections have been

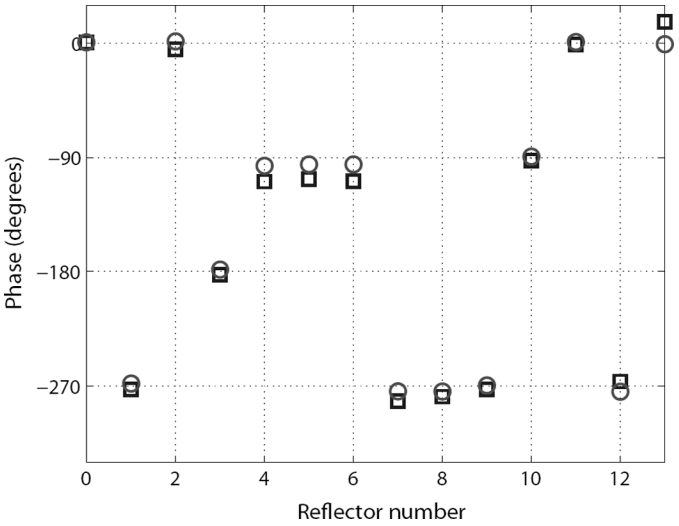

Fig. 13. Simulated (circles) and measured (squares) phases for a single phase-encoded tag. With phase corrections.

performed on these data, which is the reason why the error in the measured phases increases along the reflector array. After phase calibration, the difference of measured phases (crosses in Fig. 12) is very close to that of the simulated phases.

Fig. 13 presents the phase data (simulated and experimental) for a single phase-encoded tag sample. In this case, no reference tag has been used. After phase corrections, the phase-based code can be identified without any ambiguity.

V. Conclusion

Through this experiment, we have shown that the data capacity of SAW RFID tags can be significantly enhanced by combining the time delay information of reflective echoes with phase data. In our tags, each echo has 4 possible time positions and 4 possible phases. With 10 reflectors used for encoding, this results in 10^{12} unique codes (40 bits), which is a significant improvement compared with the 10^6 distinct codes (20 bits) that may be realized when using time delays alone. In addition to the enhanced data capacity, we have achieved a low loss level of −38 dB for reflective echoes.

Extracting and interpreting the phase information of reflected signals demands precise modeling of reflectors, even in the case of tags having a relatively small number of code reflectors as those presented above. Calibration procedures, such as using a reference tag, can be employed for robust algorithms of reading phase-encoded SAW tags.

Acknowledgments

The authors are grateful to Tessonics Corporation, Windsor, Ontario, Canada, for help in producing tag samples.

References

[1] S. Lehtonen, V. Plessky, C. Hartmann, and M. Salomaa, "Unidirectional SAW transducer for GHz frequencies," in *Proc. IEEE Ultrason. Symp.*, 2003, pp. 817–820.

[2] S. Härmä, V. Plessky, C. Hartmann, and W. Steichen, "Z-path SAW RFID tag," *IEEE Trans. Ultrason., Ferroelect., Freq. Contr.*, vol. 55, no. 1, pp. 208–213, Jan. 2008.

[3] C. Hartmann, P. Brown, and J. Bellamy, "Design of global SAW RFID tag devices," in *2nd Int. Symp. Acoustic Wave Devices for Future Mobile Communication Systems*, Mar. 2004, pp. 15–19.

[4] "FEMSAW—An extremely accurate and powerful 2D FEM/BEM simulation tool for SAW devices," [Online]. Available: http://www.gvrtrade.com.

[5] H. Li, J. Wen, K. Hashimoto, T. Omori, and M. Yamaguchi, "Optimal design of an RSPUDT-based SAW filter with constant group delay," *IEEE Trans. Ultrason., Ferroelect., Freq. Contr.*, vol. 54, no. 10, pp. 1960–1964, Oct. 2007.

[6] S. Lehtonen, V. Plessky, and M. Salomaa, "Short reflectors operating at the fundamental and second harmonics on 128°$LiNbO_3$," *IEEE Trans. Ultrason., Ferroelect., Freq. Contr.*, vol. 51, no. 3, pp. 343–351, Mar. 2004.

[7] L. Reindl and I. Shrena, "Wireless measurement of temperature using surface acoustic waves sensors," *IEEE Trans. Ultrason., Ferroelect., Freq. Contr.*, vol. 51, no. 11, pp. 1457–1463, Nov. 2004.

[8] J. Kuypers, A. Randles, M. Schmidt, S. Tanaka, and M. Esashi, "MEMS-based SAW devices," in *3rd Int. Symp. Acoustic Wave Devices for Future Mobile Communication Systems*, Mar. 2007, pp. 57–68.

Sanna Härmä was born in Kotka, Finland, in 1977. She received the M.S. (Tech.) and Lic.Sc. (Tech.) degrees from the Helsinki University of Technology (TKK), Espoo, Finland, in 2001 and 2007, and a B.A. degree (in French philology) from the University of Helsinki, Helsinki, Finland, in 2007.

She has worked as a research assistant at the Laboratory of Biomedical Engineering, TKK, as a research scientist at the Materials Physics Laboratory, TKK, as a design engineer at Thales Microsonics, Sophia-Antipolis, France, and as a subject teacher in Helsinki, Finland. She is currently preparing a D.Sc. thesis on SAW RFID tags at the Department of Engineering Physics, TKK.

Wesley G. Arthur graduated in 2000 from Anderson University (Anderson, IN) with a B.A. degree in mathematics and physics. He subsequently completed an M.S. degree in physics at the University of Windsor (Windsor, ON, Canada) in 2003. Currently, he is a Ph.D. degree candidate in physics with the Center for Imaging Research and Advanced Materials Characterization at the University of Windsor.

Clinton S. Hartmann received his B.S. degree in electrical engineering from the University of Texas at Austin in 1967. In 1968 and 1969, he received his S.M. and E.E. degrees from the Massachusetts Institute of Technology at Cambridge. In 1976, he was named the Outstanding Young Electrical Engineer in the United States by Eta Kappa Nu, the electrical engineering honor society. He is a member of Tau Beta Phi, Eta Kappa Nu, and Sigma Xi.

Mr. Hartmann began his career in 1969 at Texas Instruments, Dallas, TX, where he later

achieved the rank of TI Fellow for his pioneering work in the field of surface acoustic wave devices and applications. During this period, he invented numerous SAW devices, including the SAW resonator, which has become the most widely used SAW device in the world. In 1979, Hartmann co-founded RF Monolithics, Inc., Dallas, TX, a SAW device company that subsequently became a successful public company. In 1985, Hartmann founded Hartmann Research, Inc., Dallas, TX, where he invented and developed SAW device types, including the EWC/SPUDT, a filter commonly used in television sets and cell phones. Hartmann is currently president of RF SAW Inc., Dallas, TX, which he founded in 1998. RF SAW is leader in the design and development of SAW-based radio-frequency identification (RFID) technology and product solutions for supply chain, asset management, security, and government organization applications worldwide. During his 30-year career, Hartmann has invented many SAW devices that are in common use today. Hartmann holds more than 80 U.S. patents plus numerous international patents. He has published in approximately 80 publications. His current research interests focus on Global RFID SAW devices and physics.

Roman Gr. Maev was born in 1945 in Moscow, USSR. He received combined B.S. and M.Sc. degrees in theoretical solid-state physics from Moscow Physical Engineering Institute in 1969, and a Ph.D. degree in the theory of semiconductors in 1973 from the Physical N. Lebedev Institute of the USSR Academy of Sciences, Moscow, USSR. In 2001, he received a Dr.Sc. degree from the Russian Academy of Sciences, Moscow, Russian Federation, and in 2005, he received a full professor diploma in physics from the Russian Federation Government.

In 1978, Dr. Maev was appointed as an associate professor, and beginning in 1979 he served as acting chair of the Applied Physics and Biomedical Physics Chair at the Moscow Physics Technical Institute (University). In 1984, he established and led the Biophysical Introscopy Laboratory at N. Semenov Institute of Chemical Physics, Moscow. In 1987, Dr. Maev established and became director of the Acoustic Microscopy Center (AMC) at the Russian Academy of Sciences, Moscow.

In 1995, Dr. Maev was appointed as a full faculty professor with tenure in the School of Physical Sciences at the University of Windsor, Windsor, Ontario, Canada. He established and has been the director of the Centre for Imaging Research and Advanced Material Characterization (CIRAMC) at the University of Windsor since its inception in 1997. In 2002, he was appointed as chairholder of the Daimler-Chrysler/Natural Sciences and Engineering Research Council Industrial Research Chair in Applied Solid State Physics and Material Characterization. In 2006, Dr. Maev received the rank of university professor at the University of Windsor. He is an adjunct professor at the Johns Hopkins University, Baltimore. MD. He has published more than 250 articles, various reviews, and two monographs and is the editor of several books. He holds 23 patents.

In recognition of his contribution to the development of ultrasound techniques, Dr. Maev was awarded the Pioneer Award by the American Institute of Ultrasound in Medicine in 1988. He holds a few Annual Awards for the Best Research Results from the Russian Academy of Sciences; the Centenary Ernst Abbe Medal from the World Microscopical Society, 1989; a Letter of Recognition from the Deputy Prime Minister of Canada for Research Excellence, 2001; 2002 and 2006 Award for Outstanding Research and Development from the DaimlerChrysler Corporation; awards in recognition of research and scholarship excellence from the University of Windsor, 2000, 2001, 2002, 2004, and 2005; and the 2002 Canada Innovation Summit Award in recognition of contributions to new knowledge and technical innovation. Dr. Maev is a Senior Member of IEEE and associate editor of the *IEEE Transactions on Ultrasonics, Ferroelectrics, and Frequency Control*.

Victor P. Plessky was born in Belarus in 1952. He received a Ph.D. degree from the Moscow Physical-Technical Institute in 1978 and a D.Sc. degree from the Institute of Radio Engineering and Electronics (IRE, Russian Academy of Sciences, Moscow) in 1987. He was awarded the USSR National Award for Young Scientists in 1984.

He started to work at IRE in 1978 as a junior researcher and was promoted to laboratory director in 1987. In 1991, he also worked as a part-time professor at the Patris Lumumba University, Moscow. He received the full professor title in 1995 from the Russian Government.

In 1992, Dr. Plessky joined Ascom Microsystems SA, Bevaix, Switzerland, where he worked as a SAW project manager. Since 1997, he has lectured on various SAW topics at the Helsinki University of Technology (TKK), Espoo, Finland, as a visiting professor and currently holds a docentship at TKK. In 1998, he started to work at the Neuchâtel office (Switzerland) of Thomson Microsonics (later Thales Microsonics, finally Temex), and since 2002 he has worked as a consultant.

Dr. Plessky has been engaged in research on semiconductor physics, SAW physics (new types of waves, scattering and reflection on surface irregularities, and laser generation of SAW), SAW device development (filters, delay lines, and reflective array compressors), and magnetostatic wave studies. His current interests focus on SAW physics and low-loss SAW filter development.